Corrosion behaviour of low-antimony lead alloy in sulfuric acid solution

Z.W. Chen and J.B. See*
Pasminco Research Centre, P.O. Box 175, Boolaroo, NSW 2284 (Australia)

W.F. Gillian
Pasminco Metals, 114 William Street, Melbourne, Vic. 3000 (Australia)

(Received July 13, 1993; accepted November 15, 1993)

Abstract

The influence of cooling rate immediately after solidification on the corrosion behaviour of a low-antimony lead alloy in sulfuric acid solution has been studied at: (i) fixed potentials of 1350 and 1100 mV; (ii) cyclic potentials of 1350/1100 mV. The rate of cooling had little influence on the corrosion rate. At 1350 mV, the weight loss was linear with time, probably because the weight loss was determined by diffusion of oxygen across a subcorrosion layer of constant thickness. The corrosion occurred preferentially in the interdendritic regions. By contrast, the corrosion at 1100 mV occurred uniformly at considerably lower rates and there was a parabolic relationship between weight loss and time. Increasing temperature dramatically increases the corrosion rate.

Introduction

Recently, it has been shown that considerable increases in the extent of age hardening (hardening rate and the peak and final hardnesses) of antimony–lead alloys for battery grids can be achieved through rapid cooling by quenching immediately after solidification [1]. This information provides a basis for improving the workability of low-antimony lead alloys and, hence, for reducing handling problems in battery processing.

Quantitative information is needed on the effect of rapid cooling immediately after solidification on the corrosion properties of grids. This is because positive-grid corrosion is an important life-limiting factor of lead/acid batteries [2, 3]. Accordingly, Pasminco Research Centre has conducted a research programme to determine the influence of cooling rate after solidification on the corrosion resistance of low-antimony lead alloys used in lead/acid batteries.

It is generally agreed that positive grids corrode most during charging. Hence, corrosion tests are frequently conducted at a potential of ~1350 mV (versus Hg/Hg_2SO_4) and in ~1.27 sp. gr. H_2SO_4 [2, 4, 5]. On the other hand, the changes in the corrosion layer when the battery discharges also determine the performance of lead/acid batteries [5]. These conditions have been simulated in this investigation and the results are reported in this paper.

*Author to whom correspondence should be addressed.

SSDI 0378-7753(93)01887-N

Experimental

Casting and age hardening

Experiments were performed on a Pasminco low-antimony lead alloy (S20) of the composition: Pb–1.7wt.%Sb–0.18wt.%Sn–0.23wt.%As–0.052wt.%Cu–0.019wt.%Se–0.0016wt.%S–0.013wt.%Bi [6]. The casting facility was the same as that described previously [6, 7], except for a difference in the dimensions of the mould cavity. The cast samples had dimensions of 40 mm × 12 mm × 1.5 mm. Casting, cooling and hardness testing procedures were also the same as those described elsewhere [1, 7]. The pouring temperature was 475 °C and the mould temperature was 240 °C.

Corrosion testing

A short piece of copper wire was soldered to one corner of each cast sample. During this process, the sample was wrapped with wet cotton except for the corner that was to be soldered. This procedure greatly reduced heat flow into the sample. The copper connection was insulated with a tape of polytetrafluorethylene (PTFE).

Experiments were conducted using an Electrosynthesis model 415 potentiostat/galvanostat controller and model 420X power supply. The corrosion cell was placed in a Thermoline water-heated bath to control the temperature of the electrolyte. Two samples were used for each test and were connected together as the working electrode. Pure-lead strips with exposed areas of about 30 cm^2 were employed as the counter electrode. Potentials were measured against a $Hg/Hg_2SO_4/1.27$ sp. gr. H_2SO_4 reference electrode. The solution was prepared by adding 96 ml of 98% H_2SO_4 to 304 cm^3 of distilled water.

Corrosion tests were run using the following two conditions:

(i) *Fixed*:
potential: 1350 or 1100 mV.
temperature and time: 35 °C for up to 5 days; 70 °C for up to 1 day.

(ii) *Cyclic*:
35 °C:
- 1 cycle = 1350 mV (1 day) → 1100 mV (1 day)
- 1.5 cycles = 1350 mV (1 day) → 1100 mV (1 day) → 1350 mV (1 day)

70 °C:
- 1 cycle = 1350 mV (2.5 h) → 1100 mV (2.5 h)
- 1.5 cycles = 1350 mV (2.5 h) → 1100 mV (2.5 h) → 1350 mV (2.5 h)

Each sample was used for only one experimental point. Before testing, each sample was weighed to an accuracy of 0.001 g with an AND FX-400 electronic balance. After each test, the sample was rinsed with water and the corrosion product was stripped off in an ultrasonic cleaner using a solution of 10 g l^{-1} hydrazine dihydrochloride, 20 g l^{-1} mannitol and 100 g l^{-1} sodium hydroxide in distilled water [8]. After stripping, the sample was again weighed to determine the weight loss. The corroded thickness was calculated from the following equation:

$$h = W/(\rho_{Pb} A) \quad (1)$$

where h is the corroded thickness, W the weight loss, ρ_{Pb} the density of lead (taken as the density of the alloy), and A the exposed area.

The metallographic procedure is basically the same as that described previously [7]. In order to observe the corrosion layer, however, the samples were only slightly polished as the corrosion layer was preferentially etched.

Results and discussion

Age hardening

Age hardening curves for both air-cooled and quenched samples of the alloy are plotted in Fig. 1. Each point in the Figure is the average of three readings. Although the age-hardening behaviour of the alloy is the same as that observed in an earlier study [1], the actual values of hardness (particularly for the air-cooled sample) are slightly higher. This is because the cast samples used here were considerably thinner and were subjected to a higher cooling rate due to the more rapid loss of heat to the mould.

Effect of cooling rate on corrosion rate

Figures 2 and 3 show corrosion as a function of time for fixed potentials of 1350 and 1100 mV, respectively. Table 1 lists the corrosion results for tests using cyclic potentials. The data are for tests conducted at both 35 and 70 °C.

At fixed potentials (Figs. 2 and 3), no significant differences in corrosion rate were observed between the air-cooled and quenched alloy samples, especially for tests conducted at 1100 mV. When cyclic potentials were used, it was found that a higher cooling rate after solidification does not exert a marked influence on the corrosion rate. It could be argued, however, that the limited data do show a slight decrease in corrosion of the quenched samples. Hence, although fast cooling after solidification results in a considerable increase in precipitation hardening, it has little effect on the corrosion properties of the alloy under the experimental conditions used in this investigation.

Typical microstructures of the cast samples are presented in Fig. 4. The micrographs show that the air-cooled and quenched samples have the same cast equiaxed dendritic morphology. As expected, the number and size of precipitates is higher and smaller, respectively, for quenched samples. Clearly, this cannot be determined by optical microscopy. The identical cast structure is expected as both air-cooled samples and quenched samples were made using the same solidification conditions.

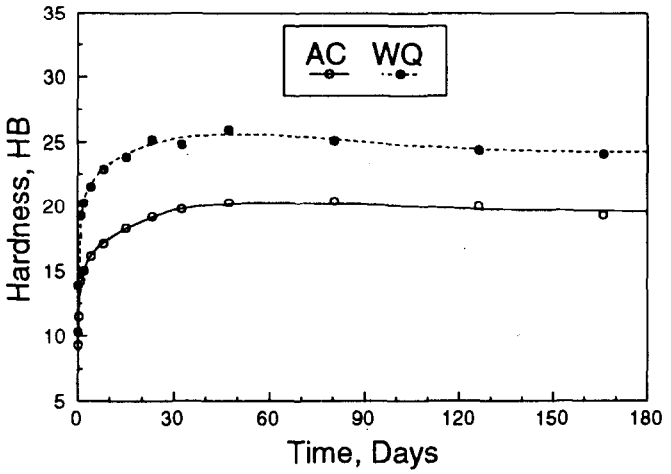

Fig. 1. Hardness curves for low-antimony lead alloy when cast and aged naturally (~22 °C). The solid curve (AC) is for samples air cooled after casting. The dashed curve (WQ) is for samples water quenched after casting.

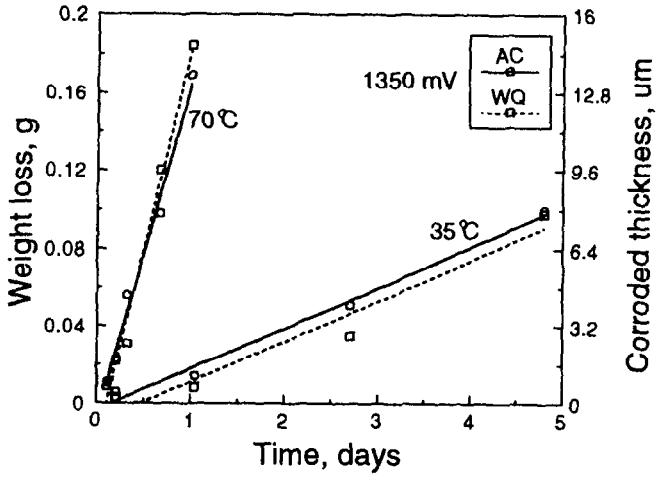

Fig. 2. Weight loss for low-antimony lead alloy samples polarized at 1350 mV in 1.27 sp. gr. H_2SO_4.

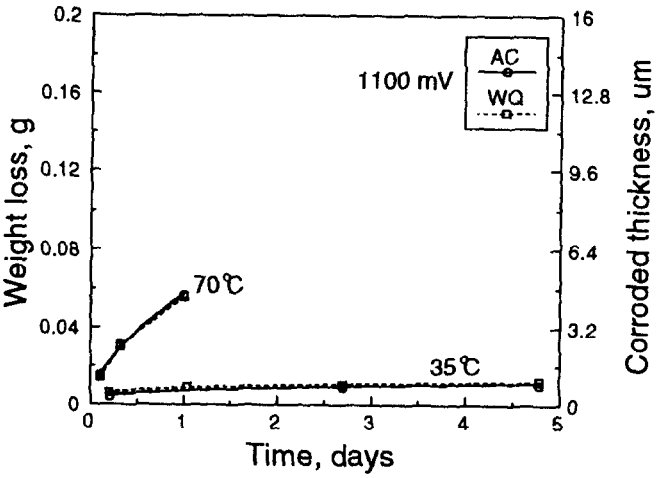

Fig. 3. Weight loss for low-antimony lead alloy samples polarized at 1100 mV in 1.27 sp. gr. H_2SO_4.

As will also be noted in the following, the morphologies of the corrosion layers formed on the air-cooled samples are identical to those formed on the quenched samples. This observation further strengthens the conclusion that the form of the precipitates has little influence on the overall corrosion behaviour.

Effect of potential and temperature on corrosion rate

From Figs. 2 and 3, it is clear that, for the same temperature, the corrosion rate is dramatically higher for tests conducted at 1350 mV than at 1100 mV. At the higher potential, an approximately linear corrosion–time relationship is observed. Under these

TABLE 1

Weight loss (g) of alloy samples under cyclic potentials (1350/1100 mV)

Temperature (°C)	1 cycle		1.5 cycles	
	AC[a]	WQ[b]	AC[a]	WQ[b]
35	0.015	0.015	0.029	0.025
70	0.014	0.013	0.033	0.025

[a]AC; air cooled.
[b]WQ; water quenched.

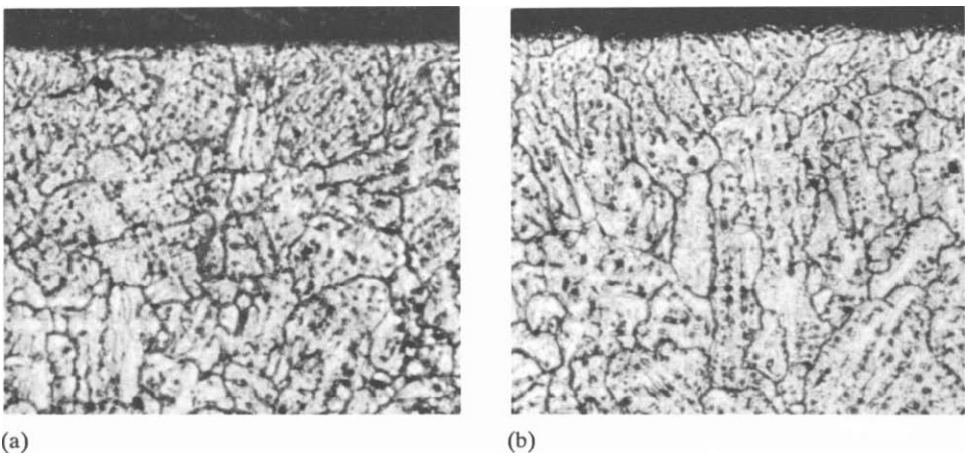

(a) (b)

Fig. 4. Microstructure of cast alloy, ×150. Structures are basically well-defined, equiaxed dendritic: (a) quenched sample, and (b) air-cooled sample.

conditions, the corrosion layer is likely to be PbO_2 with PbO present between the PbO_2 and the substrate [5, 9], although non-stoichiometric oxides could also be present [9]. For antimony–lead alloys, antimony can partially substitute for lead in the oxides [10].

The linear rate of weight loss indicates that both the flux (J) of oxygen across the corrosion layer to the substrate/corrosion-layer interface and the rate of formation of PbO at the interface are constant. It has been suggested [5, 11] that the flow of oxygen species controls the rate of PbO formation and a constant flux of oxygen results if the thickness of the layer is constant. This layer can be the overall corrosion layer or a sublayer.

Bullock and Butler [5] found that the thickness of the PbO was about 4 μm and that this thickness was relatively insensitive to either the applied potential or the temperature. If diffusion occurs through this PbO layer, and if the PbO_2 layer is porous and hence represents no barrier to diffusion, a constant rate of weight loss will result.

The considerably higher rate of weight loss observed at 70 °C may occur simply because diffusion follows Arrhenius-type behaviour. The activation energy for diffusion is estimated according to:

$$dW/dt = A_0 J = -A_0 D(dC/dX) = -A_0 D_0 \exp(-Q/RT)(dC/dX) \quad (2)$$

where dW/dt is the weight loss rate (the slope of the line in Fig. 2), t the time, J the flux, D the diffusion coefficient, dC/dX the concentration gradient (taken as approximately constant), Q the activation energy (J mol^{-1}), R the gas constant (8.314 J mol^{-1} K^{-1}), and T the absolute temperature.

Using the values of the two slopes for the two temperatures in Fig. 2, Q is estimated to be ~ 53 kJ mol^{-1}. As a comparison, Hameenoja *et al.* [11] reported values of $87 \pm 6, 29 \pm 3, 32 \pm 17$ kJ mol^{-1} for pure lead, Pb–0.85wt.%Sb and Pb–2.4wt.%Sb, respectively. These authors used rotating electrodes in sulfuric acid solution (5.35 mol kg^{-1}) saturated with oxygen and, to estimate the activation energies, measured the change in current density due to the growth of the oxide layer.

Figures 5 and 6 show the morphology of the corrosion layer formed on air-cooled samples at 1350 mV. The following features are observed.

(i) Corrosion occurs preferentially in the interdendritic (eutectic) regions at the sample surface. The depth of this penetration is between half and one dendrite grain. The penetration appears to be 'stopped' by the next grain underneath.

(ii) The morphology of the corrosion layer is the same for both 35 and 70 °C, although a thicker layer is formed at the higher temperature.

Identical features were observed on quenched samples of the alloy.

It was also found (see Figs. 5(b), 6(b)) that there is a corrosion sublayer that is chemically different (etched out) from both the substrate and the outer corrosion layer. This layer is approximately 4 to 5 μm in thickness and is present in the corrosion samples tested at both 35 and 70 °C. The layer is probably the PbO layer identified by Bullock and Butler [6]. As mentioned above, these authors noted that the thickness of the PbO layer was relatively insensitive to either the applied potential or the temperature.

A different mode of corrosion is observed when the applied potential is lowered to 1100 mV. At 35 °C, the weight loss increases very slowly with time (Fig. 3). This suggests that a passivation layer is formed which almost suppresses further corrosion. As shown in Fig. 7, the corrosion layer is very thin. At 1100 mV and 70 °C, a significantly

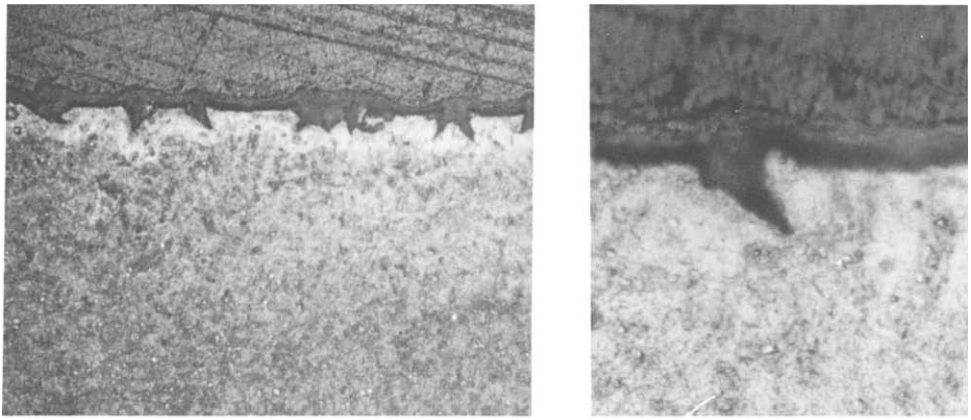

(a) (b)

Fig. 5. Micrographs of corrosion layer formed on air-cooled samples of low-antimony lead alloy polarized at 35 °C and 1350 mV for 4.8 days. Magnification (a) ×150, and (b) ×500.

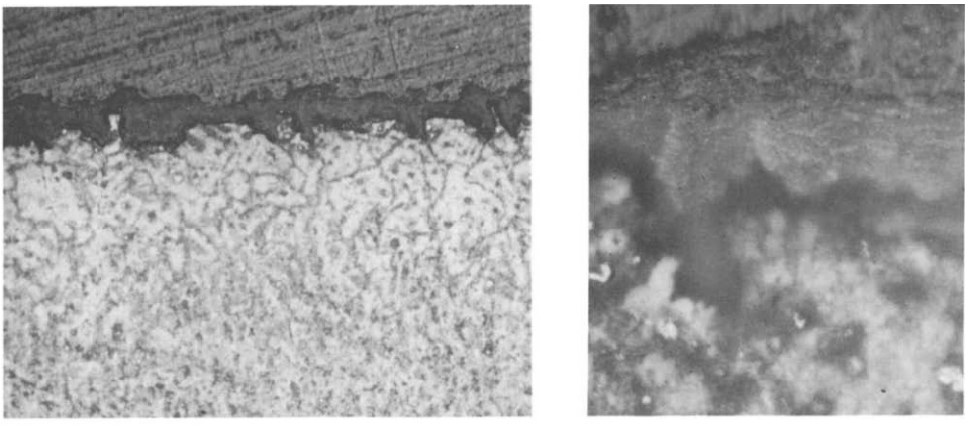

(a) (b)

Fig. 6. Micrographs of the corrosion layer formed on air-cooled samples of low-antimony lead alloy polarized at 70 °C and 1350 mV for 1 day. Magnification: (a) ×150, and (b) ×750.

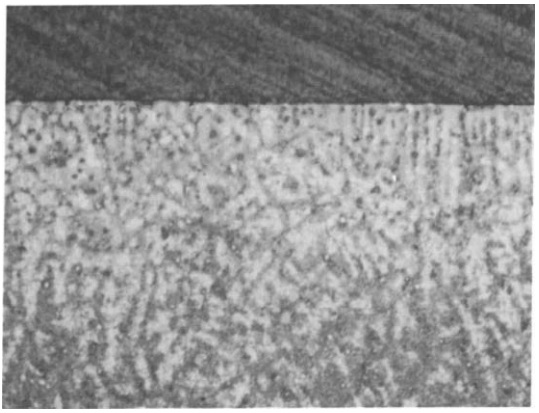

Fig. 7. Micrograph of corrosion layer formed on low-antimony lead alloy polarized at 35 °C and 1100 mV for 4.8 days. Magnification: ×150. (Note: corrosion layer is very thin.)

higher rate of weight loss is found (Fig. 3). Accordingly, the resulting corrosion layer is considerably thicker (Fig. 8). The morphologies of the corrosion layer (Figs. 7 and 8) are the same for both air-cooled and quenched samples.

Replotting the data as $(\text{weight loss})^2$ versus time yields a linear relationship for both temperatures (Fig. 9). It should be noted that the extremely small corrosion rate for the tests conducted at 35 °C prevents precise assessment at this temperature. The linearity shows that the rate of corrosion is parabolic with time and this, in turn, simply implies that the rate of corrosion is controlled by diffusion across the thickening corrosion layer. The significantly higher rate of corrosion at 70 °C is due to the fact that the diffusion across the corrosion layer follows the Arrhenius law.

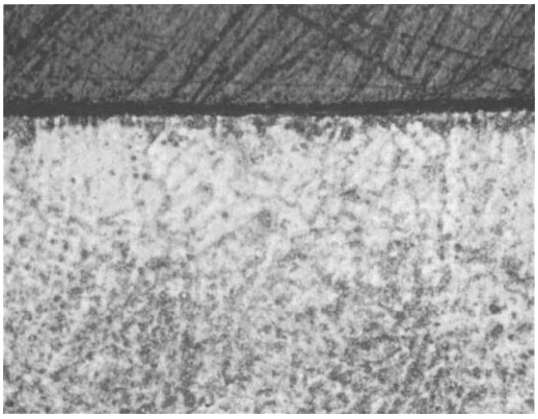

Fig. 8. Micrographs of corrosion layer formed on low-antimony lead alloy polarized at 70 °C and 1100 mV for 1 day. Magnification: ×150. (Note: corrosion layer is considerable thicker than that formed at 35 °C.)

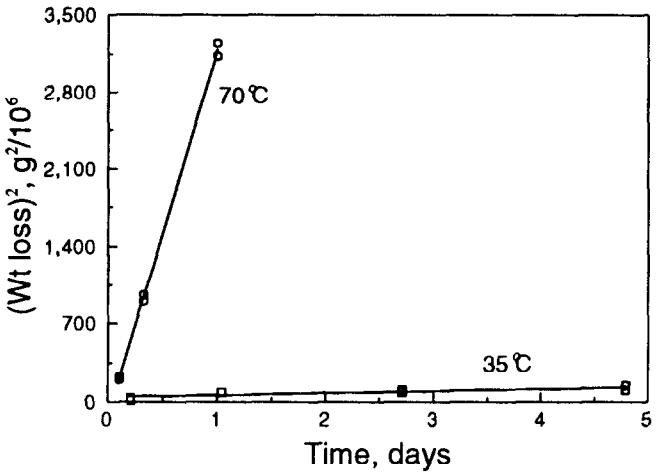

Fig. 9. (Weight loss)^2 as a function of time for low-antimony lead polarized at 70 °C and 1100 mV. (Replotting data in Fig. 3.)

Conclusions

1. The considerably higher cooling rate obtained by water quenching compared with air cooling does not significantly influence the corrosion rate of low-antimony alloys in 1.27 sp. gr. H_2SO_4 solution.

2. At 1350 mV, the rate of corrosion is linear with time at both 35 and 70 °C. The rate is very much higher at 70 °C. This may be because diffusion of oxygen is limited by a PbO layer that has a constant thickness. The considerably higher rate of corrosion at the higher temperature may be because diffusion in the PbO layer with a constant thickness follows Arrhenius-type behaviour.

3. At 1350 mV, the corrosion takes place preferentially in the interdendritic (eutectic) regions and the depth of the penetration is about the same order as the sizes of the equiaxed dendritic grains.

4. At 1100 mV, a uniform corrosion layer is formed. The growth of the layer is controlled by diffusion and the thickness increases parabolically with time. The corrosion rate and the thickening of the corrosion layer obey Arrhenius's law, i.e., the corrosion rate is considerably higher at a higher temperature.

Acknowledgements

The authors would like to thank the senior management of Pasminco Metals and Pasminco Research Centre for permission to publish this paper.

References

1 W.F. Gillian and D.M. Rice, *J. Power Sources, 38* (1992) 49–57.
2 K. Peters and N.R. Young, *Institution of Chemical Engineers Symposium Series No. 98,* Rugby, War., UK, 1986, pp. 203–215.
3 B. Culpin and D.A.J. Rand, *J. Power Sources, 36* (1991) 415–438.
4 D. Kelly, P. Niessen and E.M.L. Valeriote, *J. Electrochem. Soc., 132* (1985) 2533–2538.
5 K.R. Bullock and M.A. Butler, *J. Electrochem. Soc., 133* (1986) 1085–1090.
6 Z.W. Chen, J.B. See, W.F. Gillian and D.M. Rice, *J. Power Sources, 40* (1992) 225–234.
7 Z.W. Chen, J.B. See, W.F. Gillian and D.M. Rice, *J. Power Sources, 42* (1993) 35–45.
8 J.J. Lander, *J. Electrochem. Soc., 105* (1958) 289–292.
9 D. Pavlov and Z. Dinev, *J. Electrochem. Soc., 127* (1980) 855–863.
10 D. Pavlov and B. Monahov, *J. Electroanal. Chem., 305* (1991) 57–72.
11 E. Hameenoja, T. Laitinen, G. Sundholm and A. Yli-Pentti, *Electrochim. Acta, 34* (1989) 233–241.